Formation of α-Eucryptite, $LiAlSiO_4$: An In-Situ Synchrotron X-ray Powder Diffraction Study of a High Temperature Hydrothermal Synthesis

P. Norby*

Department of Chemistry, University of Oslo, P.O. Box 1033, Blindern, N-0315 Oslo, Norway

J. C. Hanson

Chemistry Department, Brookhaven National Laboratory, Upton, New York 11973

A. N. Fitch and G. Vaughan

European Synchrotron Radiation Facility, 38043 Grenoble, France

L. Flaks

National Synchrotron Light Source, Brookhaven National Laboratory, Upton, New York 11973

A. Gualtieri

Dipartimento Scienze della Terra, University of Modena, I-41100 Modena, Italy

Received January 27, 2000

Hydrothermal conversion of zeolite Li-A(BW), $LiAlSiO_4 \cdot H_2O$, into α-eucryptite, $LiAlSiO_4$, occurs at temperatures above 350 °C. We report here the first in-situ study of a high-temperature hydrothermal synthesis using time-resolved powder diffraction. The following hydrothermal reactions were studied: 4 M $NaNO_3$:$LiAlSiO_4$ [ABW] → Li(Na)$AlSiO_4 \cdot H_2O$ [ABW] → $Na_6Al_6Si_6O_{24} \cdot 2NaNO_3$ [SOD]; 2 M LiCl:$LiAlSiO_4 \cdot H_2O$ [ABW] → α-$LiAlSiO_4$; 2 M LiCl:$LiAlSiO_4$[ABW] → $LiAlSiO_4 \cdot H_2O$ [ABW] → α-$LiAlSiO_4$. The hydrothermal syntheses were performed in stainless steel capillaries. To maintain hydrothermal conditions, a hydraulic pressure of 2−300 atm was applied. Synchrotron X-ray radiation with energies of 35−40 keV was used in order to penetrate the steel capillaries. Room temperature Imaging Plate powder diffraction data were collected on a sample of zeolite Li-A(BW) contained in a steel capillary in an aqueous solution at 200 atm. pressure. With the use of a 10 min exposure, it was possible successfully to refine the crystal structure of zeolite Li-A(BW) using Rietveld refinement. Angle dispersive time-resolved in-situ powder diffraction patterns were collected using a Translating Imaging Plate (TIP) camera. Crystallization and degradation curves for the high-temperature hydrothermal conversion experiments were determined using integrated intensities of selected diffraction lines. The kinetic curves were analyzed using first-order rate expressions.

Introduction

Hydrothermal conversion of zeolites is an alternate route for preparation of zeolites and other aluminosilicate materials.[1−6] Conventionally, amorphous gels are used as starting material in hydrothermal syntheses of zeolites. By using crystalline starting materials, novel zeolitic materials or materials with improved purity and crystallinity can be prepared. A reduced nucleation rate for solution mediated hydrothermal crystallization is obtained as the surface area of the crystalline starting material is small compared to amorphous precursors.[1] This can result in larger crystallites being formed, as in the synthesis of single crystals of zeolite Li-A(BW), $LiAlSiO_4 \cdot H_2O$.[2,7]

Zeolite Li-A(BW) can be prepared by hydrothermal conversion of zeolite Na-LTA using $LiCl_{(aq)}$ at temperatures from ∼200−350 °C. A number of polymorphs of $LiAlSiO_4$ can be prepared from zeolite Li-A(BW) by thermal or hydrothermal transformation.[8] Anhydrous Li-ABW and γ-eucryptite can only be prepared by dry heating, while α-eucryptite forms exclusively at hydrothermal conditions. The high-temperature hydrothermal

(1) Norby, P. *J. Am. Chem. Soc.* **1997**, *119*, 5215−5221.
(2) Norby, P.; Nørlund Christensen, A.; Krogh Andersen, I. G. *Acta Chem. Scand.* **1986**, *A40*, 500−506.
(3) Barrer, R. M.; Hinds, L.; White, E. A. *J. Chem. Soc.* **1953**, 1466−1475
(4) Khodabandeh, S.; Davis, M. E. *Chem. Commun.* **1996**, *10*, 1205−1206.
(5) Zones, S. I.; Nakagawa, Y. *Stud. Surf. Sci. Catal.* **1995**, *97*, 45−52.
(6) Chiyoda, O.; Davis, M. E. *Microporous Mesoporous Mater.* **1999**, *32*, 257−264.
(7) Krogh Andersen, E.; Ploug-Sørensen, G. *Z. Kristallogr.* **1986**, *176*, 67−73.
(8) Norby, P. *Zeolites* **1990**, *10*, 193−199.

10.1021/cm991210h CCC: $19.00
Published on Web 04/26/2000

polymorph of $LiAlSiO_4$ is α-eucryptite. α-Eucryptite is one of the few naturally occurring lithium-bearing minerals, and has a phenacite/willemite type structure.[9] At even higher temperatures *β*-eucryptite is formed, which structurally can be described as a stuffed derivative of quartz.[10]

Studies of crystallization kinetics in hydrothermal syntheses are important for understanding nucleation and crystallization mechanisms as well as for understanding mineral formation. Knowledge of crystallization kinetics and occurrence of intermediate phases is also important in rational syntheses of new materials, for modification of chemical/physical properties of materials and in materials design. In the last years, a number of studies have shown that in-situ powder diffraction using synchrotron X-ray radiation is a very valuable tool for studying e.g. crystallization and chemical reactions involving crystalline material (see e.g. ref 11 and references herein as well as refs 1 and 12−15). Use of intense synchrotron X-ray radiation combined with position sensitive or area detectors enables studies of even quite fast chemical reactions, and allows real-time structural information to be extracted.[16,17]

The hydrothermal reactions in this study were performed at temperatures up to 350 °C. To maintain hydrothermal conditions a pressure equal to or higher than the water vapor pressure of the reaction mixture is required. This can be obtained from autogenous pressure, when the whole reaction vessel is heated to the desired temperature, and the pressure is provided by the water vapor. This is usually the case when hydrothermal syntheses are performed in the laboratory. Another approach is to apply a known hydrostatic pressure to the reaction mixture. We have used the second approach for in-situ studies of hydrothermal synthesis and hydrothermal conversion of zeolites and related materials using 0.5−1 mm quartz glass capillaries as reaction chambers.[1,12−14,16,17] To maintain hydrothermal conditions in the heated zone, a nitrogen pressure is applied to the surface of the reaction mixture. Only a small zone is heated, keeping the liquid/gas interface cold in order to reduce evaporation. We have used up to 45 atm pressure inside the capillaries, corresponding to a maximum temperature for maintaining hydrothermal conditions of ca. 260 °C. To obtain hydrothermal conditions at 350 °C, a pressure above 165 atm is necessary. This puts severe limitations on the container material. The reaction cell must be able to withstand the high pressure and at the same time be chemically inert toward aqueous solutions at 350°. At these temperatures, water and aqueous solutions become aggressive and reactive. When performing hydrothermal syntheses in steel vessels, iron impurities are often present in the synthesized material. However, many hydrothermal syntheses can be performed using stainless steel containers, especially when the pH is close to neutral.

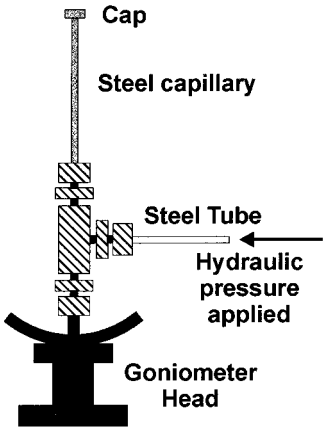

Figure 1. Sketch showing the steel capillary mounted on a goniometer head. The steel tube attached to the Swagelock T-piece is filled with water, and a hydrostatic pressure of 2−300 atm is applied using a hydraulic pump.

When performing in-situ powder diffraction studies using X-ray radiation, it is necessary to be able to penetrate the reaction cell and obtain diffraction patterns from the materials inside. By using high-energy X-ray radiation from a synchrotron source the absorption is dramatically reduced. Also, the high intensity of the X-ray beam ensures that even though part of the incoming and diffracted beam is absorbed, there is still enough diffracted intensity to obtain powder diffraction patterns with the necessary time resolution. The efficiency of collecting powder diffraction patterns is greatly enhanced by using position sensitive or area detectors, where the full powder diffraction pattern is collected simultaneously.

The aim of the present study was to study the hydrothermal conversion of zeolite Li-A(BW) to α-eucryptite at temperatures above ∼350 °C. Synchrotron X-ray radiation with energies of 35−40 keV was combined with a Translating Imaging Plate (TIP) camera developed especially for time-, temperature-, and wavelength-dependent powder diffraction experiments.[17]

Experimental Section

Phase pure and well crystalline zeolite Li-A(BW), $LiAlSiO_4 \cdot H_2O$, was prepared according to ref 2, using p.a. quality chemicals. Dehydration at 400 °C produced anhydrous Li-ABW, $LiAlSiO_4$, as described in ref 8.

The hydrothermal syntheses were performed in 70 mm long steel tubes with a outer diameter of 1.6 mm (1/16 in.) and a wall thickness of 0.3 mm. The tubes were closed in one end using a cap, and were filled with the dry lithium aluminosilicates. The starting material was then soaked with aqueous solutions of LiCl or $NaNO_3$ using a syringe. The steel tube was attached to a Swagelok T-piece mounted on a goniometer head as shown in Figure 1. The T-piece and the steel capillary containing the sample were completely filled with the aqueous solution in order to minimize changes in the concentration due to diffusion during the experiment. The steel tube was connected to the hand operated hydraulic pump and was filled completely with water. To be able to maintain a hydrostatic

(9) Roy, R.; Roy, D.; Osborn, E. F. *J. Am. Ceram. Soc.* **1950**, *39*, 145−146.
(10) Pillars, W. W.; Peacor, D. R. *Am. Mineral.* **1973**, *58*, 681−690.
(11) Cheetham, A. K.; Mellot, C. F. *Chem. Mater.* **1997**, 2269−2279.
(12) Norby, P. *Mater. Sci. Forum* **1996**, *128−131*, 147−152.
(13) Norby, P.; Nørlund Christensen, A.; Hanson, J. C. In *Studies in Surface Science and Catalysis*; Weitkamp, J., Karge, H. G., Pfeifer, H., Hölderich, W., Eds.; Elsevier: Amsterdam, 1994; Vol. 84, pp 179−186.
(14) Norby, P.; Nørlund Christensen, A.; Hanson, J. C. *Inorg. Chem.* **1999**, *38*, 1216−1221.
(15) Barnes, P.; Turrillas, X.; Jupe, A. C.; Colston, S. L.; O'Connor, D.; Cernik, R. J.; Livesey, P.; Hall, C.; Bates, D.; Dennis, R. *J. Chem. Soc., Faraday Trans.* **1996**, *92*, 2187−2197.
(16) Norby, P.; Poshni, F. I.; Grey, C. P.; Gualtieri, A. F.; Hanson, J. C. *J. Phys. Chem. B.* **1998**, *102*, 839−856.
(17) Norby, P. *J. Appl. Crystallogr.* **1997**, *30*, 21−30.

pressure throughout the experiment it is very important to avoid air bubbles in the system. Using the hydraulic pump a water pressure of 2−300 atm was applied to the steel tube containing the sample. The sample was heated using a hot air blower.[18] As the heat conductivity of the steel capillary is significant, the size of the hot air stream was ∼10 mm while the horizontal size of the beam was 2 mm. This minimizes effects from temperature gradients across the sample, which must be considered significant at the edges of the heated zone.

Time-resolved powder diffraction experiments were performed at BM16, ESRF and at X17B1, NSLS. At the powder diffraction beam line BM16 at ESRF, Grenoble[19] the X-rays from the bending magnet source are collimated vertically by a rhodium-coated silicon mirror before they are incident on the double crystal monochromator. A Si 111 reflection was used to select an X-ray energy of ∼35 keV.

Subsequent experiments were performed at the beamline X17B1 at NSLS, Brookhaven National Laboratory using ∼38 keV X-ray radiation from a superconducting wiggler. The X-rays were monochromatized using a double Si 220 crystal.

The capillary was mounted horizontally and was oscillated 90−160°. In both experiments the size of the X-ray beam was approximately 2 (horiz.) × 0.3 (vert.) mm^2 and was centered on the capillary. The vertical size of the beam was kept smaller than the diameter of the capillary in order to increase angular resolution, especially at low angles, and to decrease the ratio between the intensity of the diffraction peaks from the capillary and the sample.

For both the experiments at ESRF and NSLS, the detector used was a Translating Imaging Plate (TIP) system developed especially for time-, temperature-, and wavelength-dependent powder diffraction.[17] The TIP camera consists of an imaging plate which is translated behind a lead covered steel plate with a 3 mm vertical slit. Thereby a continuous series of powder diffraction patterns is recorded. A 200 × 400 mm flexible Fuji Imaging plate was used, and a Fuji BAS2000 scanner was used to scan the imaging plates. The imaging plate was positioned 590 and 648 mm from the sample for the experiments performed at ESRF and NSLS, respectively. The wavelength, sample−detector distance, imaging plate tilt angle and the zero point were determined using a powder diffraction pattern of LaB_6 (NIST#660) as described in ref 17. The wavelength was determined to be 0.3570(2) and 0.3224(4) Å for the experiments at ESRF and NSLS, respectively. Because of the small wavelength the powder diffraction pattern is compressed, and high angular resolution is necessary to resolve diffraction peaks. In the present geometry using a flat imaging plate the full width at half maximum (FWHM) of the diffraction peaks was between 0.025 and 0.035° in 2θ, which was sufficient to give a well-resolved powder diffraction pattern. The time resolution and data quality obtained at ESRF and NSLS were comparable.

Temperature Calibration. When performing hydrothermal syntheses in steel capillaries, where only a small zone is heated, the temperature at the actual sample position must be determined under as realistic conditions as possible. Heat transfer in the steel capillary and the solution give rise to large temperature gradients, which means that the temperature of the hot air heating the capillary must be higher than the temperature intended for the hydrothermal synthesis. The temperature at the sample position can be determined either by using thermal expansion (of for instance silver) or by observation of well-defined phase transformations or melting points. For the experiments at X17B1 the melting point of bismuth was used to determine a temperature calibration curve. Although this gives only one point on the calibration curve, the melting point of Bi (271 °C) is close to the temperature where the hydrothermal synthesis is performed. To obtain the temperature determination under realistic hydrothermal conditions, the metal was filled into a 0.5 mm capillary, which was then sealed using a flexible seal. The capillary was then inserted into the steel capillary, which was filled with water. The flexible seal ensures that as the pressure in the reaction chamber was increased, the bismuth metal is kept dry, while at the same time the heat transport conditions are very close to the actual hydrothermal conditions during the synthesis. By increasing the temperature, and at the same time measure the diffraction pattern of Bi using the TIP camera, the melting point could be observed as the diffraction lines disappear. The calibration showed, that a temperature of the hot air stream of 434 °C was necessary to obtain a sample temperature of 271 °C. Linear extrapolation indicates that the temperature of the air stream should be 565 °C to reach a sample temperature of 350 °C.

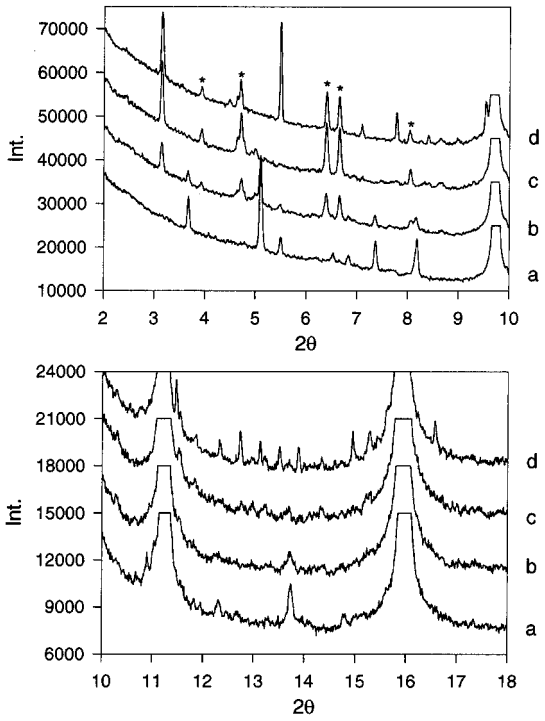

Figure 2. Imaging plate powder diffraction profiles extracted during hydration and hydrothermal transformation of anhydrous Li-ABW, $LiAlSiO_4$, in $NaNO_{3(aq)}$. Diffraction peaks from the steel contained has been truncated for clarity: (a) starting material, (b) partly hydrated two phase mixture, (c) hydrated Li(Na) ABW, and (d) partially converted sample; mixture of sodalite and zeolite ABW (marked with asterisks).

Results and Discussion

Li-ABW + $NaNO_{3(aq)}$. In Figure 2 results from in-situ hydrothermal conversion of anhydrous Li-ABW, $LiAlSiO_4$, with 4 M $NaNO_3$ are shown. The sample was contained in a steel capillary under 150 atm hydraulic pressure and was heated from room temperature to 300 °C. Figure 2, diagram A, shows the diffraction pattern of anhydrous Li-ABW, $LiAlSiO_4$, at room temperature in a ∼4 M aqueous solution of $NaNO_3$ measured at BM16, ESRF. The diffraction lines from steel are dominating the pattern, and have been cut for clarity. At room temperature no appreciable ion exchange takes place.

Several features are notable as the heating progresses. The first step in the reaction is a hydration of Li-ABW to zeolite Li-A(BW), which does not occur at ambient conditions.[8] When zeolite Li-A(BW) is dehydrated, the 8-ring channel narrows and elongates allowing the Li

(18) Argoud, P. R.; Capponi, J. J. *J. Appl. Crystallogr.* **1984**, *17*, 420−425.
(19) Fitch, A. N. *Mater. Sci. Forum* **1996**, 128−131, 219−222.

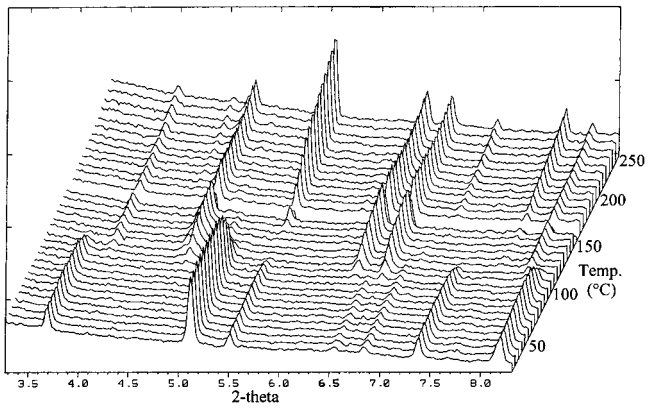

Figure 3. Three-dimensional representation of the reaction of anhydrous Li-ABW with 4 M $NaNO_{3\ (aq)}$. A small part of the diffraction pattern is shown as a function of time, and the rehydration of the zeolite and the hydrothermal conversion into the sodalite phase are clearly visible.

ion to coordinate tetrahedrally across the channel. This hinders rehydration, even by submerging in water, and only by using hydrothermal conditions is it possible to obtain the hydrated zeolite.[8] In Figure 2, diagram B, a mixture of anhydrous Li-ABW and hydrated zeolite Li-A(BW) is found. Figure 2, diagram C, shows the in-situ powder pattern of rehydrated zeolite Li-A(BW). After rehydration a slight shift in reflection positions is observed due to partial ion exchange with the Na^+ ion in solution. Zeolite Li-A(BW) does not easily undergo ion exchange,[20] but by using hydrothermal ion exchange it is possible to obtain almost fully ion exchanged materials with alkali metal and silver cations.[21] Shortly after rehydration of zeolite Li-A(BW) another phase is formed. This phase could be indexed based on a cubic unit cell with $a = 9.024(2)$ Å (21 reflections indexed), indicating a sodalite-type material. The powder pattern of the mixture of zeolite ABW and the new sodalite phase is shown in Figure 2, diagram D, where the reflections from zeolite Li-A(BW) have been marked with asterisks. Figure 3 shows a three-dimensional representation of the development of the powder diffraction patterns when heating anhydrous Li-ABW in $NaNO_{3(aq)}$.

The formation of a sodalite-like phase is surprising, as nitrate usually favors formation of cancrinite-like phases.[22] The unit cell is relatively large, which indicates that the sodalite phase formed is salt-bearing, i.e., an approximate composition $Na_6Al_6Si_6O_{24}{\cdot}2NaNO_3$. The unit cell is similar to the unit cell for Na/CrO_4−sodalite.[23,24]

The total reaction may be written as (not balanced):

$$LiAlSiO_4\ [ABW] \rightarrow Li(Na)AlSiO_4{\cdot}H_2O\ [ABW] \rightarrow Na_6Al_6Si_6O_{24}{\cdot}2NaNO_3\ [SOD]$$

Zeolite Li-A(BW) + $LiCl_{(aq)}$. By using zeolite Li-A(BW) as starting material, hydrothermal conversion

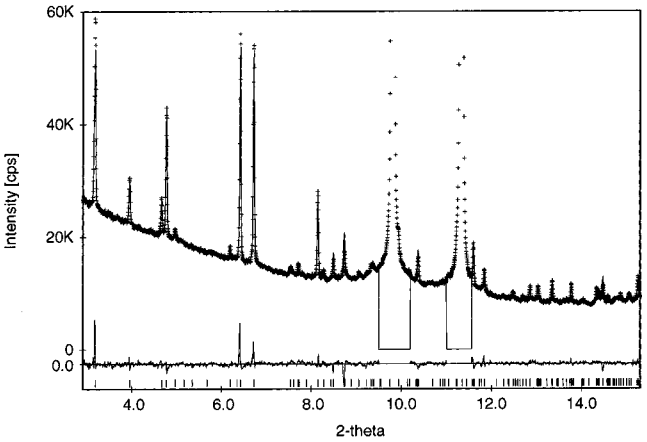

Figure 4. Observed, calculated, and difference powder diffraction patterns of zeolite Li-A(BW) in a ∼4 M LiCl solution in a steel capillary at room temperature under 200 atm hydraulic pressure. Two excluded regions are defined around the diffraction peaks from the steel capillary. Observed fwhm are between 0.025 and 0.035° 2θ.

to α-eucryptite using aqueous LiCl (∼4 M) was studied:

$$LiAlSiO_4{\cdot}H_2O\ [ABW] \rightarrow \alpha\text{-}LiAlSiO_4$$

Structure Refinement of Zeolite Li-A(BW). To investigate how much structural information it is possible to extract from powder diffraction patterns of materials under hydrothermal conditions in steel capillaries, a room-temperature powder pattern of the starting material, zeolite Li-A(BW) was obtained. The zeolite was immersed in ∼4 M aqueous solution of LiCl in a steel capillary at room temperature with an applied pressure of 200 atm. Imaging plate powder diffraction data were collected at BM16, ESRF, using an exposure time of 10 min, and a data set were extracted using a 50 pixels (5 mm) wide vertical strip.[17] The diffraction pattern was well resolved with FWHM (full width at half maximum) between 0.025 and 0.035° in 2θ. The data were rebinned to equal stepsize and corrected for geometrical effects, using the method described earlier.[17] Rietveld refinement using the program GSAS[25] was performed in the spacegroup $Pna2_1$, using the atomic coordinates from ref 2 as starting parameters. Because of the high background and decrease of the intensity of the reflections at higher angles, only data up to 15.6° in 2θ was used ($\sin\theta_{max}/\lambda = 0.421$). Two excluded regions around the diffraction peaks from the steel capillary were used. The refinement progressed smoothly, and soft constraints on the Al−O, Si−O, and Li−O distances were gradually released. Figure 4 shows the observed, calculated, and difference profiles after the final refinement. The diffraction lines from steel have been truncated. Although some discrepancies are observed between the observed and calculated pattern, the refinement was encouraging. The final agreement factors are between 1 and 2%. However, one of the main reasons for the low R values is the significant background, and does not reflect well the fit to the profile, where some discrepancies between the observed and

(20) Barrer, R. M.; White, E. A. D. *J. Chem. Soc.* **1951**, 1267−1278.
(21) Norby, P.; Fjellvåg, H. *Zeolites* **1992**, *12*, 898−908.
(22) Barrer, R. M.; Cole, J. F.; Villiger, H. *J. Chem. Soc. (A)* **1970**, 1523−1531.
(23) Norby, P. Unpublished results.
(24) Buhl, J. C.; Lons, J. *J. Alloys Compd.* **1996**, *235*, 41−47.
(25) Larson, A. C.; Von Dreele, R. B. *GSAS, General Structure Analysis System*; Report LAUR 86-748; Los Alamos National Laboratory; New Mexico, 1995.

Table 1. Refined Parameters for Zeolite Li-A(BW), $LiAlSiO_4 \cdot H_2O$[a]

	x	*y*	*z*	U_{iso}*100
Al	0.1553(10)	0.0753(6)	0.2513(16)	−0.1(3)
Si	0.3518(9)	0.3760(7)	0.2614(18)	0.5(3)
O1	0.0025(11)	0.1617(12)	0.2326(40)	3.2(6)
O2	0.2621(18)	0.2301(18)	0.1412(18)	1.7(5)
O3	0.1979(16)	0.0298(17)	0.5849(22)	2.7(8)
O4	0.1777(16)	−0.1071(12)	0.0841(18)	0.6(5)
O5	0.4965(21)	0.0907(14)	−0.3194(17)	0.6(5)
Li	0.1774(19)	0.6784(16)	0.2713(22)	2.0[b]

Distances and Angles

Si−		O1	1.595(7)	Al-		O1	1.734(7)
		O2	1.630(7)			O2	1.772(7)
		O3	1.625(8)			O3	1.767(8)
		O4	1.650(8)			O4	1.732(8)
O1	−Si−	O2	112.3(10)	O1	−Al−	O2	104.9(9)
O1		O3	114.2(10)	O1		O3	111.4(12)
O1		O4	106.6(12)	O1		O4	116.7(8)
O2		O3	101.0(10)	O2		O3	106.9(7)
O2		O4	108.6(7)	O2		O4	112.8(10)
O3		O4	114.1(8)	O3		O4	103.9(8)
Li-		O2	2.000(9)	Al	−O1−	Si	143.7(8)
		O3	2.005(9)	Al	−O2−	Si	140.0(8)
		O4	1.995(9)	Al	−O3−	Si	126.9(9)
		O5	1.989(9)	Al	−O4−	Si	121.4(8)
O2	−Li−	O3	111.1(9)				
O2		O4	104.3(8)				
O2		O5	124.8(10)				
O3		O4	108.5(8)				
O3		O5	104.7(10)				
O4		O5	102.4(8)				

[a] Distances are in angstroms, and angles, in degrees. Standard deviations are in parentheses. Space group: $Pna2_1$(33), a = 10.3369(4), b = 8.2125(3), and c = 5.0074(2) Å. Final agreement factors: R_{wP} = 1.3%, R_P = 1.6%, R_F^2 = 14.0%, χ^2 = 0.3, D_{dw} = 1.50. [b] Temperature factor for Li fixed.

calculated profiles are clearly seen. This is reflected in the rather high $R(F^2)$ (14%). The high background, giving a very low signal-to-background ratio, is probably also one of the reasons for the obtained value of χ^2, which is less than 1. In addition, assignment of realistic counting statistics for data obtained by imaging plates is not straightforward. The low value of χ^2 would suggest that the esd's for the data are overestimated. The discrepancies in Figure 4 cannot be explained by preferred orientation or absorption effects. No significant residual electron density was found from the difference Fourier maps in the channel. Refinement of the population of O5 (the water molecule) gave a value of 1.1. Refinement of the population of the lithium cation was possible, but did not show significant deviation from full occupancy. The thermal parameters were allowed to vary during the refinement, except for Li. The temperature factor for Si refined to a slightly negative value. Refining the thermal parameters resulted in only an insignificant improvement of the R values. Because of the limited sin θ/λ range and the difficult experimental conditions, no physical meaning can be attached to refined thermal parameters. The final parameters are listed in Table 1 together with distances and angles. The refined structure is in good agreement with published results.[2,7]

The result of the refinement is encouraging, as it means that it is possible to obtain structural information from samples encapsulated in steel capillaries, using short exposure times. In addition to in-situ studies of high-temperature hydrothermal syntheses, this will be important for studies of, for instance, working catalysts and fuel cells.

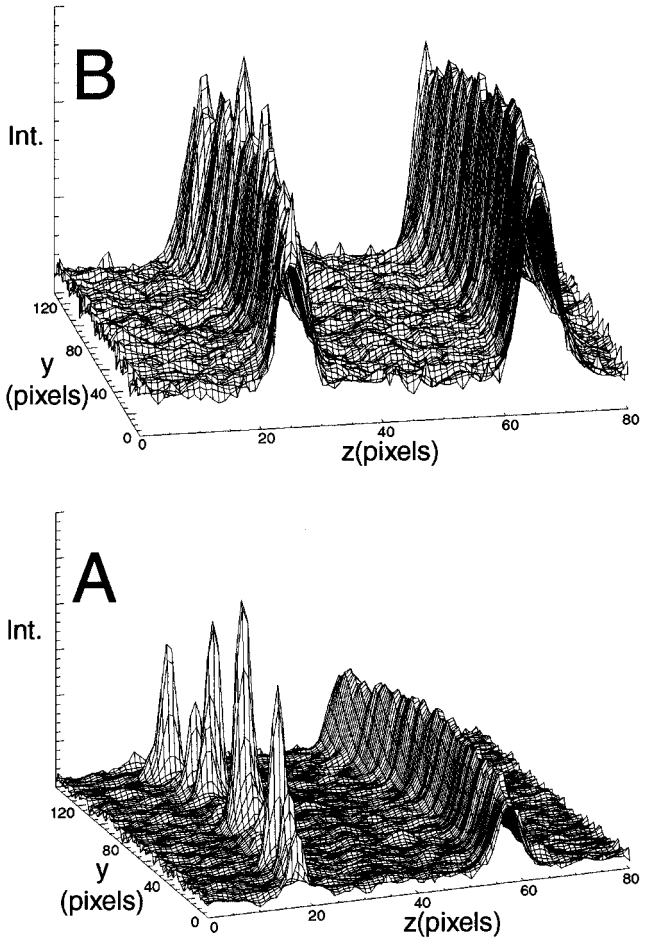

Figure 5. Three-dimensional representation of powder diffraction patterns collected using imaging plate technique. A small part of the Debye−Scherrer rings of a partially converted sample showing diffraction from the starting material, zeolite Li-A(BW), and the product, α-eucryptite. Powder diffraction patterns are shown using (a) no oscillation of the sample, and (b) using a 160° oscillation.

In-Situ Hydrothermal Synthesis. The zeolite Li-A(BW)/4 M LiCl-sample was heated slowly, and the onset of hydrothermal conversion was observed when the temperature reached 425 °C (temperature of the hot air stream). According to the literature[2,8] the hydrothermal conversion starts at ∼350 °C. The temperature gradient through the sample container is therefore significant because the thermal conductivity of the steel capillary will cause heat to disperse.

Figure 5 shows part of the Debye−Scherrer rings of the starting material and the formed α-eucryptite. The figures show three-dimensional representations of small parts of the imaging plate, and the axes are the y and z directions given in pixels.[17] In Figure 5a the pattern was obtained without oscillation of the sample, and a clear difference is seen between the Debye Scherrer rings. The starting material is a powder with very small crystallites, and consequently the Debye−Scherrer ring is uniform and smooth. The product, α-eucryptite, grows as larger crystals, and the result is Debye−Scherrer rings which consists of a number of sharp reflections as seen from Figure 5a. To follow the synthesis, integrated intensities of diffraction lines is used to estimate

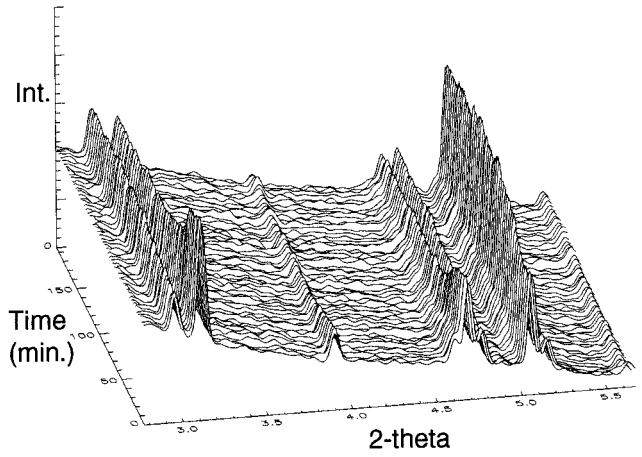

Figure 6. Three-dimensional plot showing the time dependence of a small part of the powder diffraction pattern during partial hydrothermal conversion of zeolite Li-A(BW) into α-eucryptite.

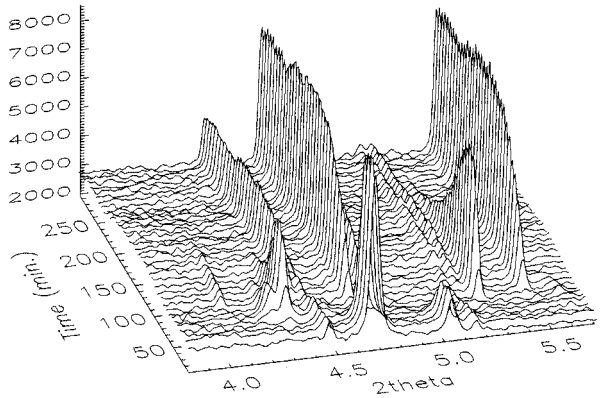

Figure 7. Three-dimensional plot showing a series of powder patterns during hydrothermal hydration of $LiAlSiO_4$ to $LiAlSiO_4 \cdot H_2O$ and the subsequent transformation into α-eucryptite, $LiAlSiO_4$. Diffraction peaks from an intermediate polymorph of $LiAlSiO_4$, *β*-eucryptite, is seen.

the amount of crystalline material. It is therefor very important to obtain good averaging to avoid erroneous values for the integrated intensities when sampling only a small part of the Debye−Scherrer ring. By oscillation of the sample 160° a significant improvement in the averaging is obtained, as seen from Figure 5b.

Figure 6 shows a small part of the diffraction pattern as a function of time during hydrothermal conversion of zeolite Li-A(BW) to α-eucryptite. A decrease of the intensity of the starting material and the accompanying increase of the intensity of the conversion product is clearly seen.

To gain more information concerning the kinetics of the hydrothermal transformation additional in-situ high-temperature hydrothermal experiments were performed at the beam line X17B1 at NSLS. Temperature calibration was performed as described in the Experimental Section. The temperature of the hot air stream was ramped to 590 °C in 60 min and was kept at that temperature. According to the calibration curve this corresponds to a temperature inside the capillary of 365 °C. Figure 7 shows a three-dimensional representation of the powder diffraction patterns obtained. The first reaction observed is the hydration of the starting material $LiAlSiO_4$, Li-ABW, into zeolite Li-A(BW),

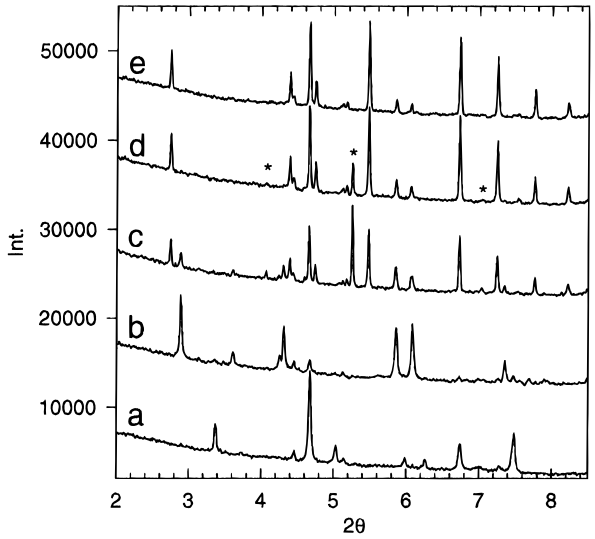

Figure 8. Separate powder patterns showing stages in the hydrothermal conversion: (a) starting material, Li-ABW, (b) zeolite Li-A(BW), (c and d) mixture of α- and *β*-eucryptite, and (e) α- eucryptite

$LiAlSiO_4 \cdot H_2O$. Transformation into α-eucryptite starts after ∼1 h, and proceeds to completion in ∼2 h. However, as seen in Figures 7 and 8, an intermediate phase is formed. This phase was only observed in some of the experiments, and it was difficult to establish the conditions leading to the formation of this phase. In Figure 8, five separate powder diffraction patterns are shown. The starting material (a) is hydrated to form zeolite Li-A(BW) (b). Then the hydrothermal transformation occurs with the last diffraction pattern (e) showing the final pure phase of α-eucryptite. In the diffraction patterns c and d, reflections from the intermediate phase are visible, marked with asterisks. A total of seven diffraction lines which did not belong to either zeolite Li-A(BW) or α-eucryptite were observed with *d* spacings: 4.54, 3.518, 2.624, 2.275, 1.909, 1.644, and 1.436 Å. From these lines the phase was identified as *β*-eucryptite, another polymorph of $LiAlSiO_4$, which has a stuffed quartz type structure. This finding is surprising, as *β*-eucryptite is a high temperature polymorph, which is usually formed[26] (hydrothermally and by dry heating) only at temperatures above 800 °C. The most likely explanation of the formation of *β*-eucryptite in the in-situ experiments is the large temperature gradient inside the steel capillary. This means that the temperature close to the surface of the capillary is higher than the temperature in the center, facilitating formation of *β*-eucryptite. However, the temperature measured in the hot air stream was below 600 °C, which may indicate that the transformation temperature decreases when a lithium chloride solution is used instead of pure water, which was used in the work described in ref 26.

The reaction followed was

$$LiAlSiO_4[ABW] \rightarrow LiAlSiO_4 \cdot H_2O\ [ABW] \longrightarrow \alpha\text{-}LiAlSiO_4$$
$$\searrow \quad \beta\text{-}LiAlSiO_4 \quad \nearrow$$

(26) Isaacs, T.; Roy, R. *Geochim. Cosmochim. Acta* **1958**, *15*, 213−217.

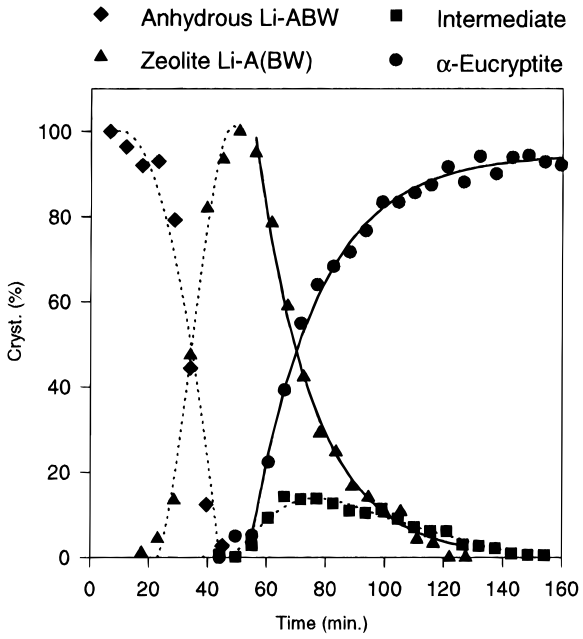

Figure 9. Crystallization and transformation curves for the four phases present during hydrothermal conversion of α-eucryptite. Integrated intensities of diffraction peaks as a function of time were used to estimate the amount of crystalline material present. For crystallization of α-eucryptite and degradation of zeolite Li-A(BW) fit to first-order rate expressions are shown.

Kinetics Analysis. Figure 9 shows the crystallization and transformation curves for the four phases present during reaction. Hydrothermal rehydration of Li-ABW into zeolite Li-A(BW) occurs at relatively low temperatures (>110 °C according to ref 8). After 45 min, the hydration reaction is complete. The curves for anhydrous Li-ABW and zeolite Li-A(BW) cross close to 50%. Finally the transformation to α-eucryptite occurs. The appearance of the intermediate phase is shown also in this figure. The scale factor for normalizing the integrated intensity of reflections from the intermediate phase was determined so that the sum of the normalized integrated intensities for the three phases was close to 100%.

The crystallization curve of α-eucryptite and the degradation curve of zeolite Li-A(BW) were fitted with first-order rate expressions:

For formation of α-eucryptite:

$$I(\%) = 100 - \exp(-k(t - t_0)),$$
$$k = 0.045(2)\ \text{min}^{-1} \text{ and } t_0 = 53.8(5)\ \text{min}$$

For degradation of zeolite Li-A(BW):

$$I(\%) = 100 - \exp(-k(t - t_0)),$$
$$k = 0.051(2)\text{min}^{-1} \text{ and } t_0 = 55.7(4)\ \text{min}$$

In Figure 9 are shown the curves obtained using first-order kinetics, and the fit is seen to be satisfactory. The rate constants and t_0 obtained for crystallization and degradation are very similar, and from the curve it is seen that the curves cross close to 50% conversion. This indicates that no appreciable amounts of amorphous phases are active in the conversion process. The intermediate β-eucryptite phase observed in some of the in-situ experiments is formed from zeolite Li(ABW) simultaneously with α-eucryptite and is seen subsequently to transforms into α-eucryptite.

The presented results demonstrates that it is possible to extract structural and kinetic information and identify intermediate phases from in-situ powder diffraction studies of high-temperature hydrothermal synthesis performed in steel capillaries. The use of high-energy synchrotron X-ray radiation is crucial in these experiments in order to penetrate the reaction chambers. The use of monochromatic radiation and angle dispersive diffraction techniques allows high-resolution powder diffraction pattern to be collected, suitable for identification as well as kinetic and structural investigations. Application of this technique is of special interest in connection with studies of high-temperature hydrothermal mineral formation.

Acknowledgment. Dr. J. Hastings and Dr. A. Frost Jensen are gratefully acknowledged for assistance with data collection at X17B1 and BM16, respectively. This work was supported under contract DE-AC02-76CH00016 with the US Department of Energy by its Division of Chemical Sciences, Office of Basic Energy Sciences, and by the Danish Natural Science Research Council.

CM991210H